Iranian Journal of Science and Technology, Transactions of Civil Engineering
https://doi.org/10.1007/s40996-025-01900-8

METHODOLOGY

The Seismic Performance of Auxetically Holed Welded Steel Connections

Oğuzhan Akarsu[1] · **Abdulkadir Cüneyt Aydin**[1]

Received: 17 February 2025 / Accepted: 6 May 2025

Abstract
This study proposes a novel welded beam-to-column connection featuring star-shaped auxetic perforations in the beam web to enhance seismic performance. A total of 27 parametrically varied finite element models were constructed to evaluate the impact of auxetic geometric parameters under FEMA-350 cyclic loading using ANSYS. The models were parametrically varied by adjusting star angle, perforation area, spacing, and the number of openings. Validation was conducted through comparison with the SJ-8 experimental connection. The results revealed significant improvements in structural behavior, particularly in terms of strength retention, ductility, rotation capacity, and energy dissipation. The top-performing configuration, ST-50-3-A-H, exhibited a peak strength of 132.79 kN, a strength degradation ratio of only 9.22%, and a ductility coefficient of 6.09, along with wide and stable hysteresis loops. These findings demonstrate that the integration of auxetic geometry into steel moment connections offers a promising strategy for improving seismic resilience. Further research is recommended to validate the proposed designs through full-scale experimental testing and to assess their practical applicability in structural engineering.

Keywords Steel · Connection · Auxetic structure · Cyclic loading · Ductility

1 Introduction

Structural engineering plays a pivotal role in safeguarding built environments by ensuring that structures can withstand both static and dynamic loads throughout their service life. As urbanization expands into seismically active zones, the discipline's emphasis has increasingly shifted toward improving structural resilience against extreme events such as earthquakes (An et al. 2018). Contemporary research focuses on enhancing the deformation capacity, energy dissipation, and post-yield behavior of critical load-bearing elements. In particular, advances in seismic design have prioritized the optimization of beam-to-column connections, which represent some of the most vulnerable points in moment-resisting frames (Hu et al. 2025; Liu et al. 2025). These efforts are supported by parallel developments in soil-structure interaction analysis, structural health monitoring, and the application of performance-based design methodologies aimed at minimizing post-earthquake damage and facilitating rapid recovery.

Steel moment-resisting frames (SMRFs) have long been favored in seismic regions due to their high ductility, superior mechanical performance, and suitability for prefabrication and rapid erection (Tsavdaridis et al. 2014). Despite these advantages, numerous studies have identified the beam-to-column joints as the most critical and failure-prone components during seismic events. Historical earthquakes such as the 1994 Northridge event and the 1995 Kobe earthquake exposed the brittle behavior of conventional welded connections, which often resulted in sudden loss of load-carrying capacity and local buckling at the beam ends (Miller 1998; Muguruma et al. 1995). These failures highlighted the insufficient plastic rotation capacity of welded joints under cyclic loads, prompting a surge of research into retrofitting and redesigning these connections to better accommodate inelastic deformation. As illustrated in Fig. 1, the failure mechanisms observed in such systems typically involve flange or web fracture at the joint region, underscoring the need for innovative connection strategies that can enhance energy dissipation and delay fracture propagation.

✉ Abdulkadir Cüneyt Aydin
acaydin@atauni.edu.tr

[1] Department of Civil Engineering, Engineering Faculty, Ataturk University, 25030 Erzurum, Turkey

Published online: 10 June 2025

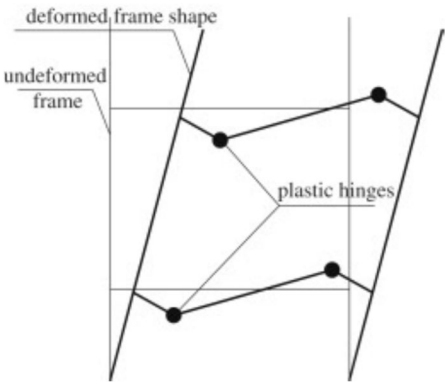

Fig. 1 Failure mode of ductile frame (Yang et al. 2009)

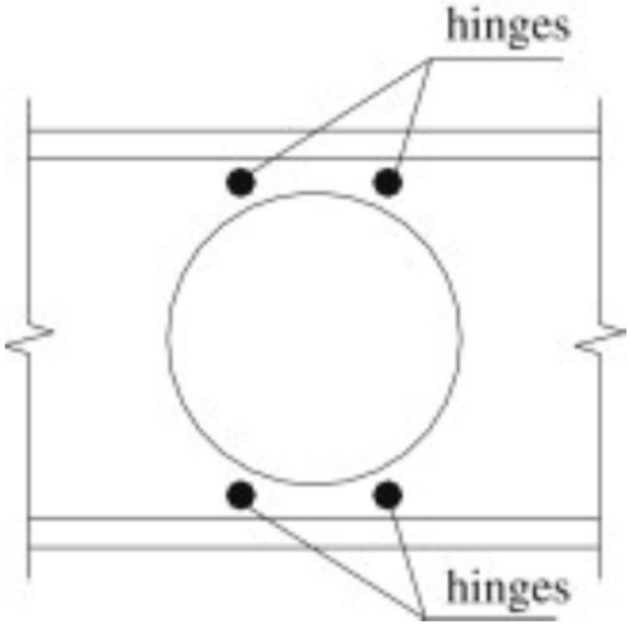

Fig. 2 Vierendeel mechanism (Yang et al. 2009)

In response to the deficiencies observed in conventional welded joints, several advanced connection strategies have been developed to improve the seismic performance of SMRFs (Yang et al. 2009). Among these, two primary methodologies have gained widespread adoption: (1) weakened connections, most notably the Reduced Beam Section (RBS), and (2) strengthened connections, including the use of cover plates or flange plates (Xu et al. 2022). The RBS technique involves intentional section cutouts in the flange or web near the beam end, thereby relocating the plastic hinge formation away from the critical weld zone at the column face. This shift reduces the likelihood of brittle fracture and facilitates stable cyclic deformation. In contrast, strengthening methods aim to increase the local stiffness and flexural strength at the beam ends through the addition of reinforcing plates, thereby delaying yielding and enhancing moment capacity. Both approaches offer improvements in energy dissipation and ductility, yet each entails distinct trade-offs in terms of fabrication complexity, cost, and compatibility with existing frame geometries.

Previous research has shown that weakening strategies—such as using reduced flange sections or introducing web openings in beams—can effectively enhance deformation capacity, minimize the likelihood of brittle fracture at beam end welds, and improve overall energy dissipation under seismic loading (Tsavdaridis et al. 2014; Xu et al. 2022; Yang et al. 2009). One common approach involves creating perforations in the beam web, which promotes the formation of Vierendeel hinges due to the combined action of bending moment and shear force (see Fig. 2) (Chung et al. 2001). Since this failure mode is generally ductile in nature, strategically placing web openings away from the beam-to-column interface can help dissipate energy and improve the inelastic behavior of moment-resisting frames. On the other hand, strengthening methods—such as the addition of flange or cover plates—have also demonstrated excellent cyclic performance by increasing local strength and stiffness at the beam ends (Zhang et al. 2019). However, these approaches often require upsizing of columns to maintain compliance with the strong-column/weak-beam design principle, which can make the overall system less economical. As such, there remains a pressing need for alternative connection strategies that offer an optimal balance between seismic resilience and structural efficiency.

To fully understand the role of Reduced Beam Section (RBS) connections in seismic design, it is important to consider the breadth of research that has explored their behavior under extreme loading conditions. RBS configurations, which involve strategic cutouts in the beam flange, have consistently demonstrated their ability to improve ductility, delay the onset of brittle failure, and enhance the energy dissipation capacity of steel frames (Mahmoud and Turbert 2014; Sofias and Tzourmakliotou 2018). Numerous numerical investigations have confirmed the efficacy of these connections in promoting stable plastic hinge formation under post-earthquake conditions. Beyond traditional RBS studies, recent work has examined the use of replaceable beam segments in accordance with established codes such as the Chinese GB50017-2014 and GB50011-2010 standards, emphasizing the modularity and reparability of seismic-resistant structures (Zhao et al. 2024). Complementary studies have addressed the complex composite action that arises in fully restrained beam-to-column connections, illustrating its impact on both strength and collapse capacity in special moment frames (Elkady and Lignos 2014). Moreover, advanced finite element modeling has enabled detailed analysis of beam web impairment strategies—such as RBS and Reduced Web Sections (RWS)—under seismic loading

scenarios (Sofias and Tzourmakliotou 2018). Experimental investigations have extended these insights by assessing RBS performance under fire exposure, revealing how elevated temperatures influence the ductility and integrity of such systems (Guo and Huang 2016). Collectively, these studies underscore the critical role of connection detailing in achieving reliable and resilient steel frame behavior across a variety of extreme conditions.

The extensive body of research on reduced beam section strategies and their implementation in steel structures has significantly enriched current understanding of connection behavior under seismic and fire-induced stresses. By integrating experimental findings, analytical models, and advanced numerical simulations, these efforts have paved the way for more resilient, repairable, and performance-based designs within modern structural engineering practice. However, despite the progress, achieving an optimal balance between seismic performance and constructability remains an ongoing challenge.

Moreover, limited research has addressed how novel geometries—such as auxetic patterns—might contribute to overcoming the inherent trade-offs between strength, ductility, and constructability in beam-to-column joints.

This study aims to develop and evaluate a novel steel beam-to-column connection design by integrating auxetic star-shaped perforations into the beam web, inspired by developments in metamaterials. These perforations, characteristic of auxetic geometry, exhibit a negative Poisson's ratio and are known for their superior shear resistance and energy absorption. Auxetic structures, known for exhibiting a negative Poisson's ratio, possess distinct mechanical traits such as increased shear resistance and superior energy absorption under repeated loading (Alomarah et al. 2022; Liu et al. 2023). These properties have been successfully utilized in fields ranging from biomedical engineering to aerospace applications, but their use in civil infrastructure, particularly steel seismic connections, remains rare and relatively uncharted.

Although auxetic geometries have demonstrated excellent mechanical performance in materials science, their structural-scale applications in welded steel connections have received limited attention. No previous study, to the best of our knowledge, has systematically examined the role of auxetic perforations in improving the seismic performance of full-scale moment connections.

To respond to the growing need for innovative, yet practical, solutions in seismic retrofitting, this study proposes a hybrid connection concept that merges flange cover plate reinforcement with auxetic-inspired web geometry. Unlike conventional designs employing Vierendeel mechanisms or standard web perforations, the proposed configuration leverages controlled deformation zones that promote distributed plasticity while minimizing stress concentrations and stiffness degradation under cyclic loads. A comprehensive parametric study was conducted using nonlinear finite element analysis in ANSYS to evaluate 27 models, each varying in geometric properties such as star angle, spacing, and number. Performance was assessed using key metrics including hysteresis shape, energy dissipation, strength degradation, and ductility capacity under loading protocols consistent with FEMA-350 standards.

The numerical investigation was conducted using nonlinear finite element modeling (FEM) in ANSYS, simulating cyclic loading in accordance with FEMA-350 protocols. Twenty-seven parametric models were analyzed, varying in star angle, area, spacing, and number of perforations. Performance indicators included hysteretic shape, strength degradation, rotation capacity, and total energy dissipation.

What distinguishes this research is its attempt to translate material-scale auxetic logic into a structural-scale application within welded steel frame systems. By doing so, it addresses a gap in current seismic design methodologies, offering a potential alternative that blends the benefits of both weakened and strengthened connection philosophies. Without imposing significant increases in member size or fabrication complexity, the proposed design has the potential to improve the overall structural efficiency of moment-resisting frames in high-seismic regions, while opening a new line of inquiry for performance-based structural metamaterial integration.

2 Auxetic Structures

Auxetic structures represent a distinctive category within the broader class of mechanical metamaterials, notable for their negative Poisson's ratio—a property whereby the material expands laterally when compressed along its axis (Wang et al. 2024). This counterintuitive deformation behavior results in a suite of advantageous mechanical properties, including enhanced shear strength, resistance to indentation and fracture, superior energy and acoustic absorption, and improved surface isotropy (Zhang et al. 2023). In contrast to conventional materials, which tend to bulge outward when compressed vertically, auxetic structures contract in the transverse direction, as illustrated in Fig. 3 (Zhang et al. 2023).

Auxetic structures have been categorized into several types based on their geometric configuration, scale of application, and underlying deformation mechanisms. These include auxetic cellular solids, molecular-scale materials, fiber-reinforced composites, and various classes of polymers (Mojaver et al. 2024). Notable geometric configurations comprise re-entrant and chiral honeycombs, double-arrowhead structures, star-shaped units, and rotating rigid or semi-rigid mechanisms—all of which exhibit distinct

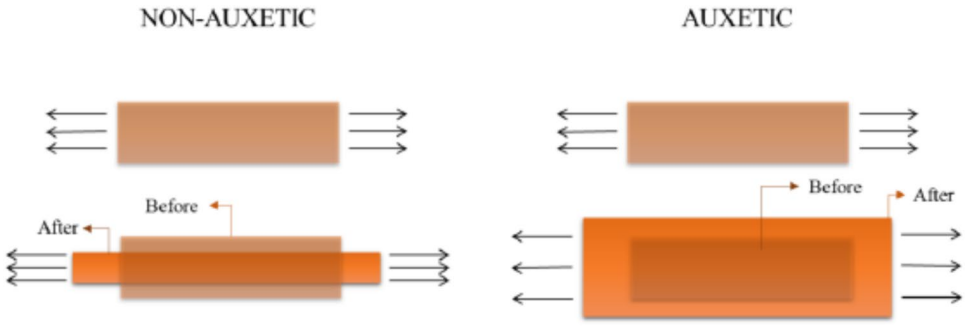

Fig. 3 Illustration depicts the behavior of auxetic and non-auxetic materials (Zhuohong 2020)

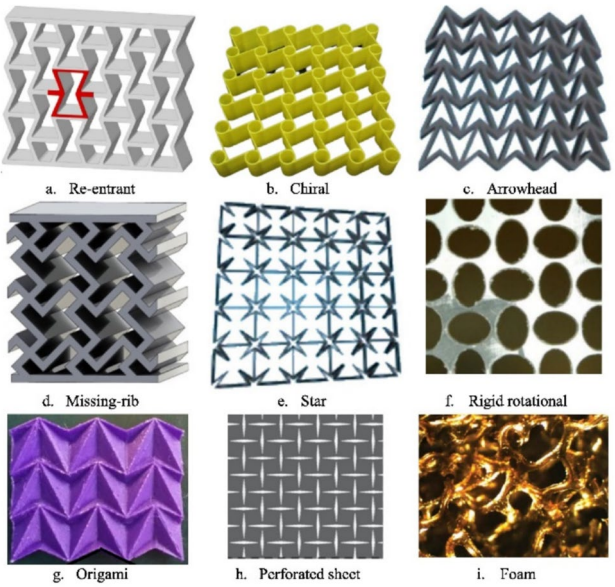

Fig. 4 Conventional auxetic structures (Bohara et al. 2023)

mechanical behaviors and deformation patterns (Alomarah et al. 2022). Owing to their tunable properties, these forms have been adapted across diverse sectors, including aerospace engineering, defense technologies, medical devices, and advanced textiles (Nguyễn et al. 2023; Rose et al. 2023; Wang and Hu 2014). Their high strength-to-weight ratio, enhanced indentation resistance, superior energy absorption, and adjustable permeability make them attractive for multifunctional design applications (Bagewadi and Bhagchandani 2023). Examples such as bioprosthetic implants, memory foams, and impact-absorbing footwear demonstrate how auxetic principles have successfully transitioned from theoretical models to real-world products (Hassanin et al. 2020). Conventional examples of such structures are illustrated in Fig. 4.

While the unique mechanical properties of auxetic materials have been well documented at the micro- and meso-scale, their application in full-scale structural components—particularly welded steel connections—remains an emerging frontier in civil engineering. In the context of this research, auxetic behavior is harnessed through star-shaped perforations introduced into the beam web, aiming to enhance seismic performance by promoting controlled energy dissipation and improved ductility. However, incorporating such geometries into welded joints raises new engineering questions, particularly concerning stress redistribution, fatigue life, and local buckling behavior under cyclic loading. As one of the earliest studies to investigate the structural-scale integration of auxetic forms in seismic steel connections, this work aims to provide a foundational understanding for future analytical and experimental efforts in this evolving domain.

Auxetic structures exhibit unique tensile responses, which are markedly different from conventional materials due to their negative Poisson's ratio and distinct deformation mechanisms. To better illustrate this behavior, stress–strain curves obtained from both analytical modeling and finite element (FE) simulations are presented in Fig. 5.

As shown in Fig. 5, the auxetic structures initially undergo a linear elastic response followed by a significant non-linear phase characterized by strain hardening. The initial phase corresponds to the bending of the inclined cell walls, leading to a progressive rotation toward the loading direction. After yielding, the structures enter a plastic deformation regime where the stress increases steadily due to strain hardening effects. The comparison between theoretical results (black solid lines) and FE results (red dashed lines) reveals a good agreement, validating the analytical approach.

It is observed that in the rigid-perfectly plastic model, after initial yielding, the stress remains relatively constant before strain hardening dominates. In contrast, when strain hardening is considered, a continuous increase in stress is evident throughout the deformation process. This behavior significantly enhances the energy absorption capacity of the auxetic structures under large tensile strains, making them promising candidates for impact mitigation and self-centering applications.

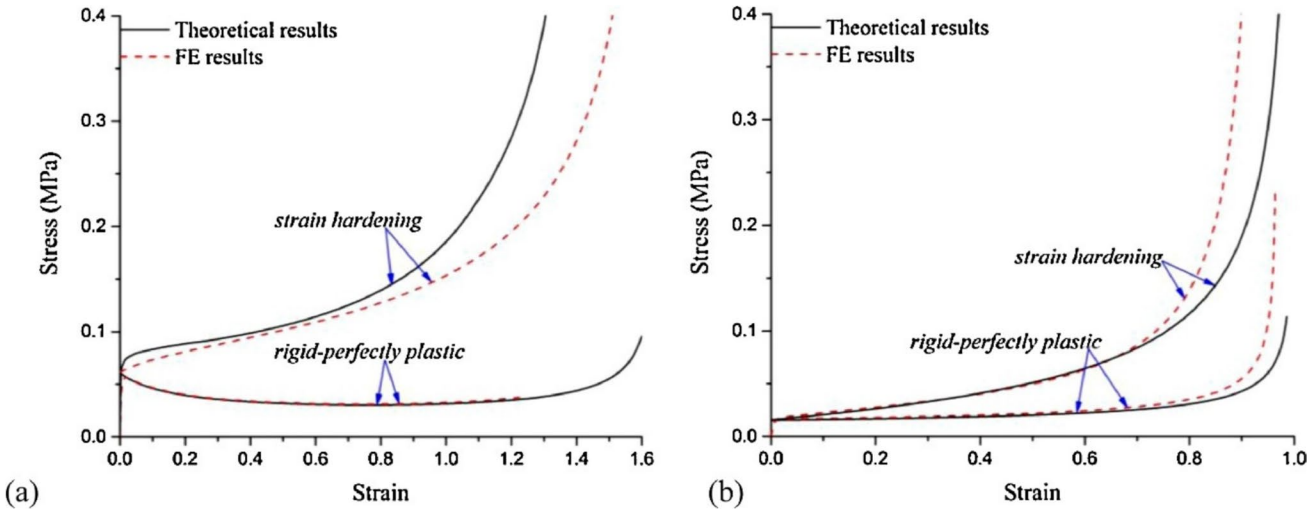

Fig. 5 Comparison of theoretical and finite element results for the tensile behavior of re-entrant auxetic structures (Zhang et al. 2018)

3 Numerical Model

This section presents the finite element modeling approach developed to simulate the seismic behavior of welded steel beam-to-column connections enhanced with auxetic perforations. The objective is to numerically investigate how variations in auxetic geometry—such as star angle, spacing, and quantity—affect key seismic performance indicators, including ductility, energy dissipation, and strength degradation. A total of 27 parametric models were created and evaluated using nonlinear finite element analysis (FEA) in ANSYS. Additionally, validation against experimental results was conducted to confirm the reliability of the simulation framework.

To verify the accuracy and reliability of the numerical simulations, the finite element results were validated against experimental data. For this purpose, the SJ-8 connection model developed by Xu et al. (2022) was used as a benchmark reference (Xu et al. 2022). The comparison focuses on replicating observed failure mechanisms, including flange and web buckling, to ensure that the numerical model accurately captures critical seismic response characteristics.

3.1 Model Details

The primary objective of this study is to propose an improved welded steel connection that maintains the original joint's strength and stiffness while facilitating the relocation of the plastic hinge away from the column face. This modification aims to reduce the risk of brittle fracture at the beam end during seismic loading. The connection consists of a welded assembly between a column with a cross-section of HW $250 \times 250 \times 9 \times 14$ mm (length: 2.05 m) and a beam with an HN $300 \times 150 \times 6.5 \times 9$ mm profile (length: 1.75 m). Although cover plates are included in the connection geometry, their parameters are not investigated as variables in this study. Instead, the cover plate dimensions are fixed at 120 mm (width), 200 mm (length), and 10 mm (thickness), in accordance with typical design practices. The geometric configuration is illustrated in Fig. 6. Furthermore, the beam-to-column stiffness ratio and the width-to-thickness ratio of the plate were designed to comply with the GB50017 Code for Steel Structures in China. The design of the flange cover plate was also guided by recommendations provided in FEMA-350 (Xu et al. 2022).

The auxetic pattern introduced into the beam web was defined using several geometric parameters, including the star's internal angle (α), surface area (A), spacing between patterns (d), and the total number of stars (n). These parameters are illustrated in Fig. 7, while the model labeling convention is described in Fig. 8. Each parametric configuration was designed to explore the influence of these variables on the overall seismic performance of the connection. The dimensional specifications of all specimen models, corresponding to their geometric variations, are provided in Table 1.

A total of 27 parametric models were developed to systematically investigate the influence of auxetic geometry on seismic performance. These models incorporate variations in star angle (α), perforation area, spacing, and quantity, enabling a comprehensive assessment of geometric parameters affecting ductility, energy dissipation, and strength degradation. While the present study adopts a broad design space to capture general behavioral trends, future research may benefit from a more targeted classification of configurations based on specific performance objectives, such as stiffness optimization or plastic rotation control.

Fig. 6 Steel welded connection

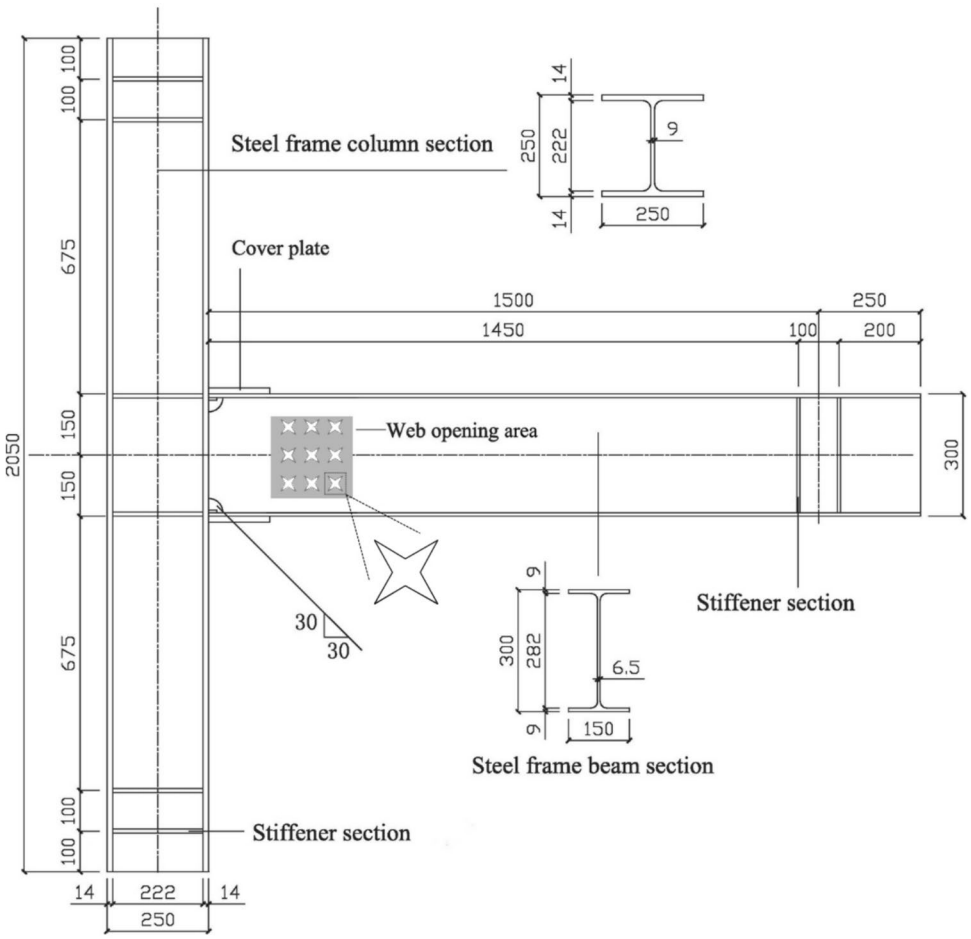

Fig. 7 Parameters of auxetic structures (α, angle of edge, L_1 and L_2, side length, d, distance of star A, area of star, n, number of star)

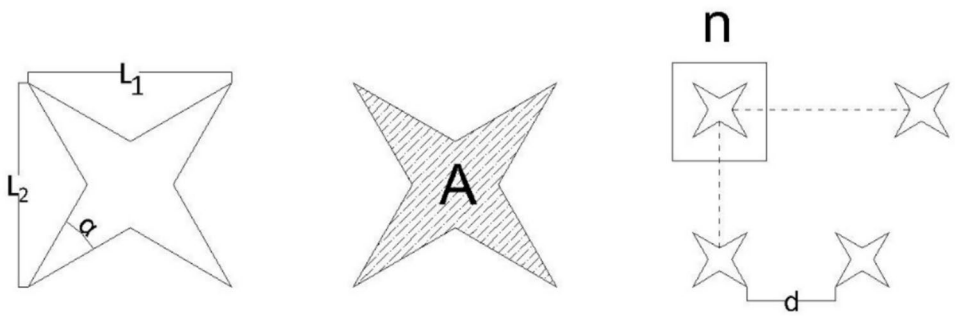

3.2 Material Properties and Boundary Conditions

A global nonlinear finite element modeling (FEM) framework was employed to analyze the hysteretic response of the proposed connection models under cyclic loading. The simulations accounted for both geometric and material nonlinearities to accurately capture the inelastic behavior of the steel components. The steel material was modeled using a multilinear isotropic hardening law, enabling the capture of both elastic and plastic deformation phases, with post-yield hardening behavior based on experimental stress–strain data. The yield surface of the material was defined using the von Mises yield criterion, which is widely accepted for modeling isotropic ductile metals under multiaxial stress states. The mechanical properties of the structural steel used in the analysis were adopted from the experimental data reported by Xu et al. (2022), ensuring consistency between the numerical model and the validation benchmark. These properties—including yield strength, ultimate strength, elastic modulus, and elongation—are summarized in Table 2.

Boundary conditions were established by fully restraining the column ends, while cyclic lateral displacements

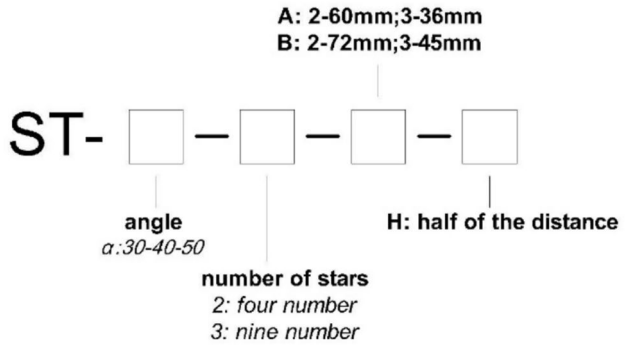

Fig. 8 Model labelling rules

were incrementally applied at the free end of the beam to simulate seismic loading conditions, as illustrated in Fig. 9. The loading protocol adhered to FEMA-350 (Venture and Guidelines Development Committee 2000) guidelines, consisting of 34 displacement-controlled cycles with increasing amplitudes (Fig. 10). The horizontal distance from the point of load application to the face of the column flange was set at 1500 mm, which is representative of typical span-to-depth ratios used in moment-resisting frame systems. This configuration was chosen to accurately replicate the deformation demands experienced by beam-to-column connections in real structural systems.

The displacement-controlled loading protocol, summarized in Table 3, consisted of ten sequential load steps designed to simulate increasing seismic demand on the connection. The initial three steps each included six load cycles, intended to represent moderate amplitude oscillations during early earthquake phases. The fourth step involved four cycles at a higher amplitude, marking the transition into inelastic deformation behavior. The remaining six steps each consisted of two cycles with progressively larger displacements, allowing for the evaluation of strength degradation, ductility, and energy dissipation capacity under severe loading conditions. This staged loading approach reflects realistic seismic excitation patterns and aligns with the FEMA-350 guidelines for evaluating cyclic performance of steel connections.

Table 1 Design parameters of connection

Model	Number of stars	α (deg0)	$L_1 = L_2$ (mm)	Distance (d) (mm)	Star area (cm^2)
ST-30-1	1	30	180	–	136.9
ST-30-2-A	4	30	60	60	60.8
ST-30-2-B	4	30	72	36	87.6
ST-30-2-A-H	4	30	60	30	60.8
ST-30-2-B-H	4	30	72	18	87.6
ST-30-3-A	9	30	36	36	49.5
ST-30-3-B	9	30	45	22.5	77.4
ST-30-3-A-H	9	30	36	18	49.5
ST-30-3-B-H	9	30	45	11.25	77.4
ST-40-1	1	40	180	–	172.9
ST-40-2-A	4	40	60	60	76.8
ST-40-2-B	4	40	72	36	110.8
ST-40-2-A-H	4	40	60	30	76.8
ST-40-2-B-H	4	40	72	18	110.8
ST-40-3-A	9	40	36	36	62.1
ST-40-3-B	9	40	45	22.5	97.2
ST-40-3-A-H	9	40	36	18	62.1
ST-40-3-B-H	9	40	45	11.25	97.2
ST-50-1	1	50	180	–	206.1
ST-50-2-A	4	50	60	60	91.6
ST-50-2-B	4	50	72	36	132
ST-50-2-A-H	4	50	60	30	91.6
ST-50-2-B-H	4	50	72	18	132
ST-50-3-A	9	50	36	36	73.8
ST-50-3-B	9	50	45	22.5	116.1
ST-50-3-A-H	9	50	36	18	73.8
ST-50-3-B-H	9	50	45	11.25	116.1

Table 2 Mechanical properties of the steel

Plate thickness (mm)	Yield strength (MPa)	Ultimate strength (MPa)	Elastic modulus (MPa)	Elongation (%)
6.5	335.23	382.81	2.06×10^5	32.66
9.0	341.38	393.62	2.06×10^5	30.79
14.0	326.64	381.58	2.05×10^5	34.17

3.3 Model Validation

The proposed finite element models were benchmarked against the experimental results of the SJ-8 welded steel connection tested by Xu et al. (2022), which served as a reference for evaluating the reliability of the simulation framework. While the comparison provides meaningful insight into the performance of auxetically holed connections, it should be noted that conventional strengthening methods—such as cover plate-only, RBS, or standard welded joints—were not included in this phase of the analysis. Future work will incorporate these traditional configurations as baseline models to facilitate a more comprehensive assessment of the relative benefits introduced by auxetic geometries.

To verify the accuracy of the finite element analysis (FEA), simulation results were compared with the experimental findings from the SJ-8 model tested by Xu et al. (2022). As shown in Fig. 11, the comparison includes the experimental setup (a) and corresponding FEA results for total deformation (b), von Mises stress distribution (c), and failure patterns (d). The tested specimen featured a column section of $HW250\times250\times9\times14$ mm and a beam section of $HN300\times150\times6.5\times9$ mm. The experimental observations revealed significant flange and web buckling under cyclic loading, which were accurately captured by the numerical model. The close correlation between experimental and simulated deformation modes affirms the robustness of the FEA framework in replicating local instability phenomena and global joint behavior under seismic demands.

To ensure the accuracy and stability of the finite element simulations, a mesh sensitivity assessment was conducted during the modeling process. The structural components were discretized using SOLID185 elements—linear, 3D structural solids capable of capturing nonlinear behavior and complex geometries. Mesh refinement was applied particularly in regions of geometric discontinuity, such as near the auxetic perforations and around the beam-to-column weld zones, where localized stress concentrations were anticipated. The global mesh was defined with an average element size of 15.0 mm, while the minimum edge length reached 6.5 mm to accurately capture fine deformation patterns. The resulting mesh quality met convergence criteria for nonlinear static analysis and ensured reliable predictions of stress and buckling responses under cyclic loading.

Fig. 9 Boundary conditions

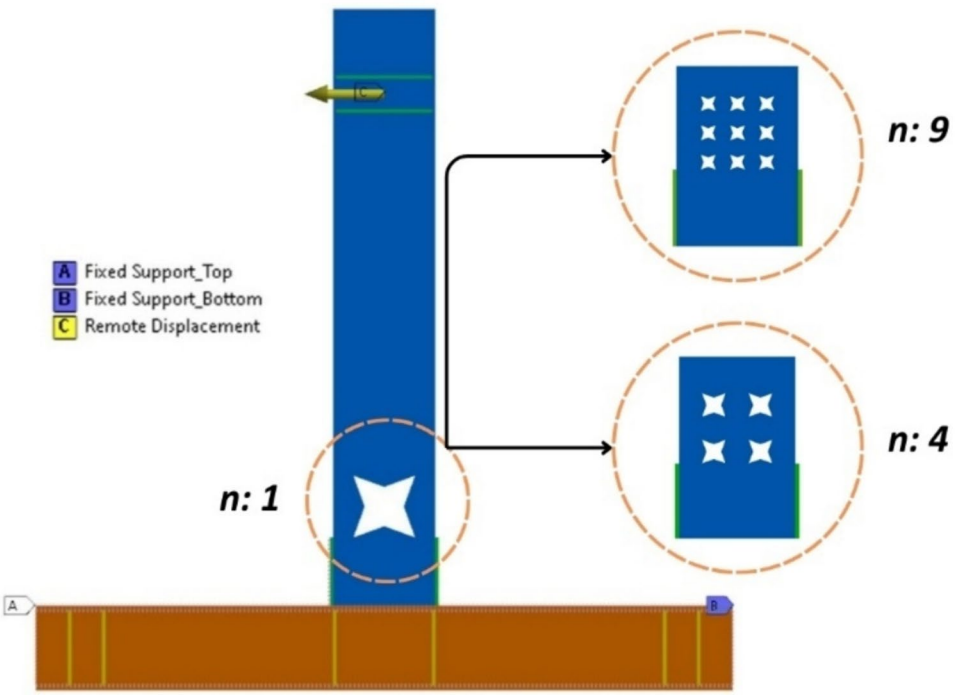

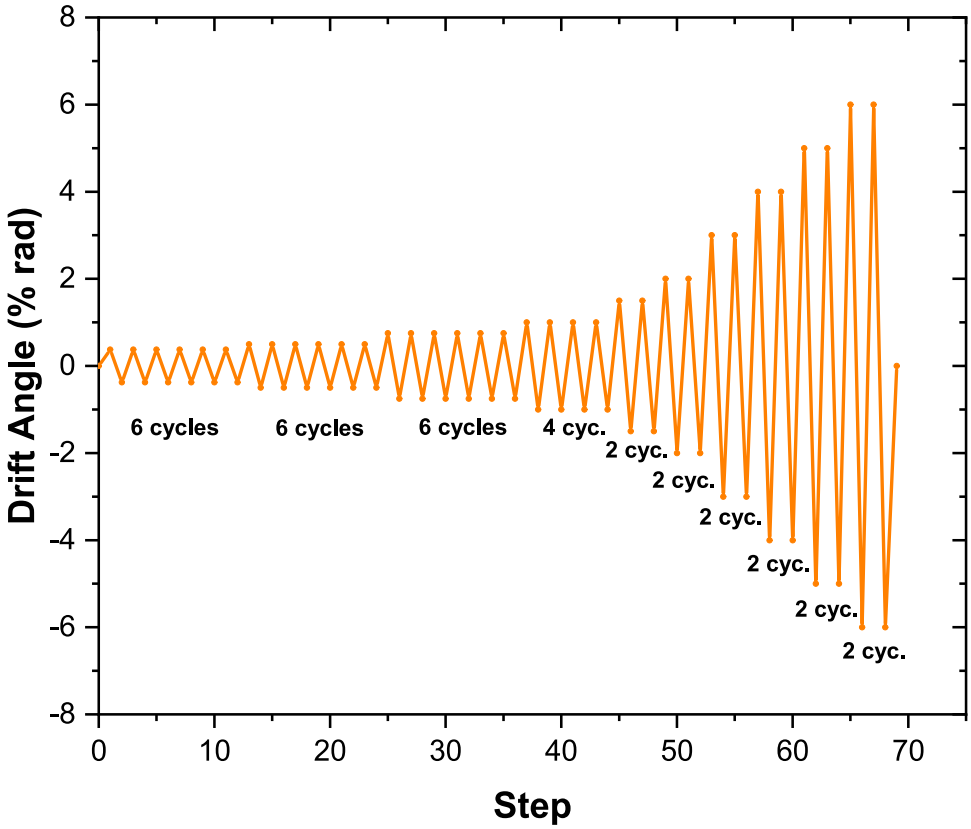

Fig. 10 Cyclic loading protocol (FEMA-350)

Table 3 Loading protocols

Load step	Lateral displacement (mm)	Number of cycles	Peak deformation (rad)
1	±5.625	6	0.00375
2	±7.500	6	0.00500
3	±11.250	6	0.00750
4	±15.000	4	0.01000
5	±22.500	2	0.01500
6	±30.000	2	0.02000
7	±45.000	2	0.03000
8	±60.000	2	0.04000
9	±75.000	2	0.05000
10	±82.500	2	0.05500

4 Results and Discussions

Among the 27 evaluated models, the configurations ST-50-3-A-H, ST-40-3-A-H, and ST-30-3-A-H exhibited superior seismic performance across multiple criteria, including load-bearing capacity, strength degradation, ductility, and hysteretic energy dissipation (see Fig. 12). The ST-50-3-A-H model, in particular, achieved the highest load capacity at 132.79 kN, coupled with the lowest observed strength degradation and a stable, full-shaped hysteresis loop—indicative of its robust cyclic performance. The ST-40-3-A-H configuration followed closely, demonstrating an impressive ductility coefficient of 6.19 and a total rotation capacity of 6.36 radians, reflecting its capability to undergo large inelastic deformations without loss of structural integrity. Similarly, ST-30-3-A-H presented a balanced combination of deformation control and energy absorption, confirming the effectiveness of the auxetic configuration at smaller star angles. Collectively, these results suggest that integrating star-shaped auxetic perforations—particularly in triple configurations with reduced spacing—can significantly enhance seismic resilience by facilitating distributed yielding and mitigating stiffness degradation in welded steel connections.

4.1 Hysteretic Behavior

The hysteretic behavior of beam-to-column steel connections plays a crucial role in determining the seismic performance of structural frames. Prior studies have underscored the importance of ductility and energy dissipation in ensuring structural resilience. Tsavdaridis and D'Mello (2012) highlighted the role of Vierendeel mechanisms in perforated beams, emphasizing the complex interaction of shear forces and localized moments. Braconi et al.

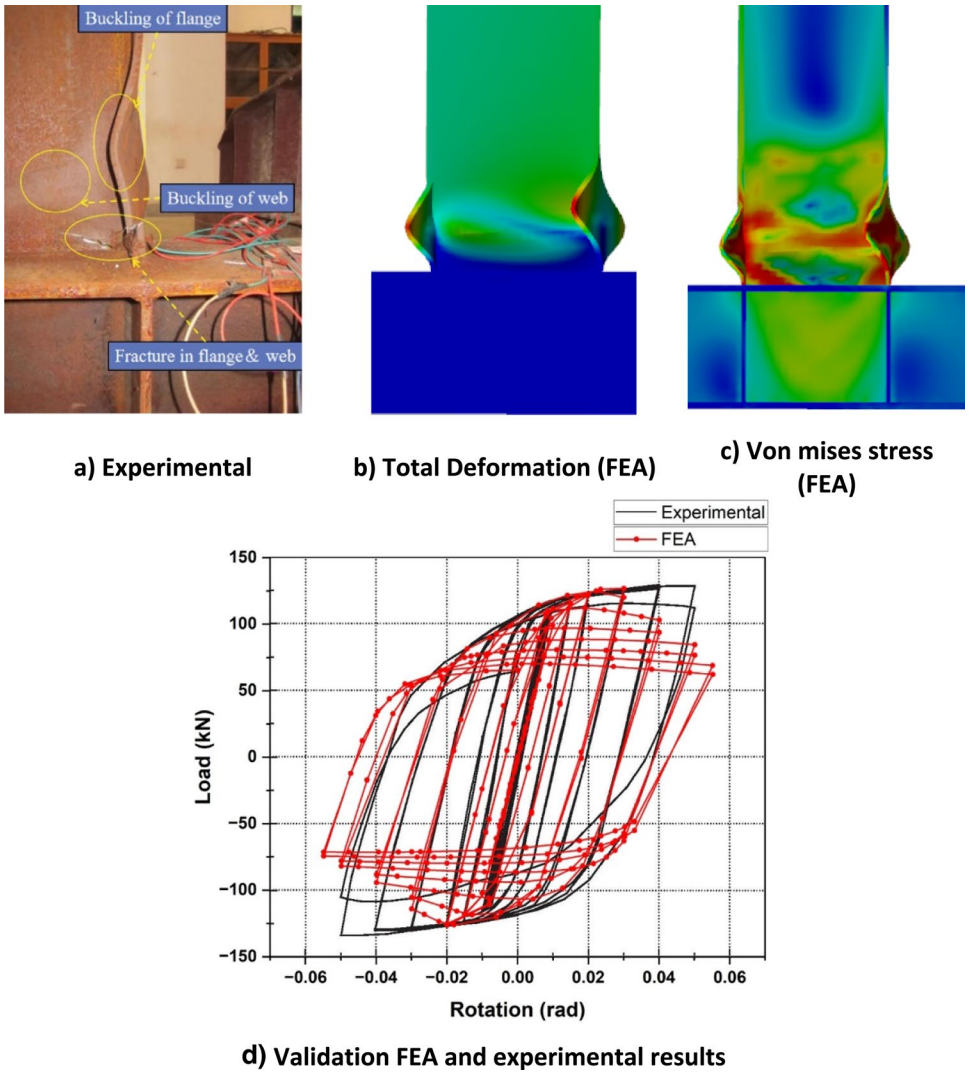

Fig. 11 Verification of FE modeling

(2007) further demonstrated the advantages of ductile partial-strength connections, which facilitate global frame mechanisms with high hysteretic energy dissipation. Similarly, Han and Li (2010), along with Bishay-Girges (2020). emphasized the necessity of rigidity in moment-resisting connections to maintain lateral stability under cyclic loading. While most of these studies focused on traditional steel configurations, Li and Huang (2022) extended this discussion to reinforced concrete joints, offering valuable insights into energy absorption and ductility through experimental hysteresis analysis.

In the context of the present study, Fig. 13 illustrates the hysteresis curves for all 27 auxetically perforated steel connection models. The curves exhibit full spindle-shaped loops without significant pinching and maintain symmetry under both positive and negative loading directions—an indication of stable cyclic behavior and high energy dissipation capacity.

It is evident that the hysteretic curves of all models exhibited a full spindle shape without the pinching phenomenon and a symmetric form in both negative and positive directions, showcasing a favorable energy dissipation capacity.

4.2 Envelope Curves

The envelope curve, constructed by connecting the peak points of each hysteresis cycle, serves as a simplified yet informative representation of a connection's overall force–displacement behavior. This curve is particularly useful for evaluating strength degradation, stiffness evolution, and ultimate capacity under repeated cyclic loading. In this study, envelope curves were generated for all parametric models to facilitate direct comparison of seismic performance indicators. As shown in Fig. 14, these curves reflect the progressive stiffness degradation and ultimate failure characteristics of the specimens. The

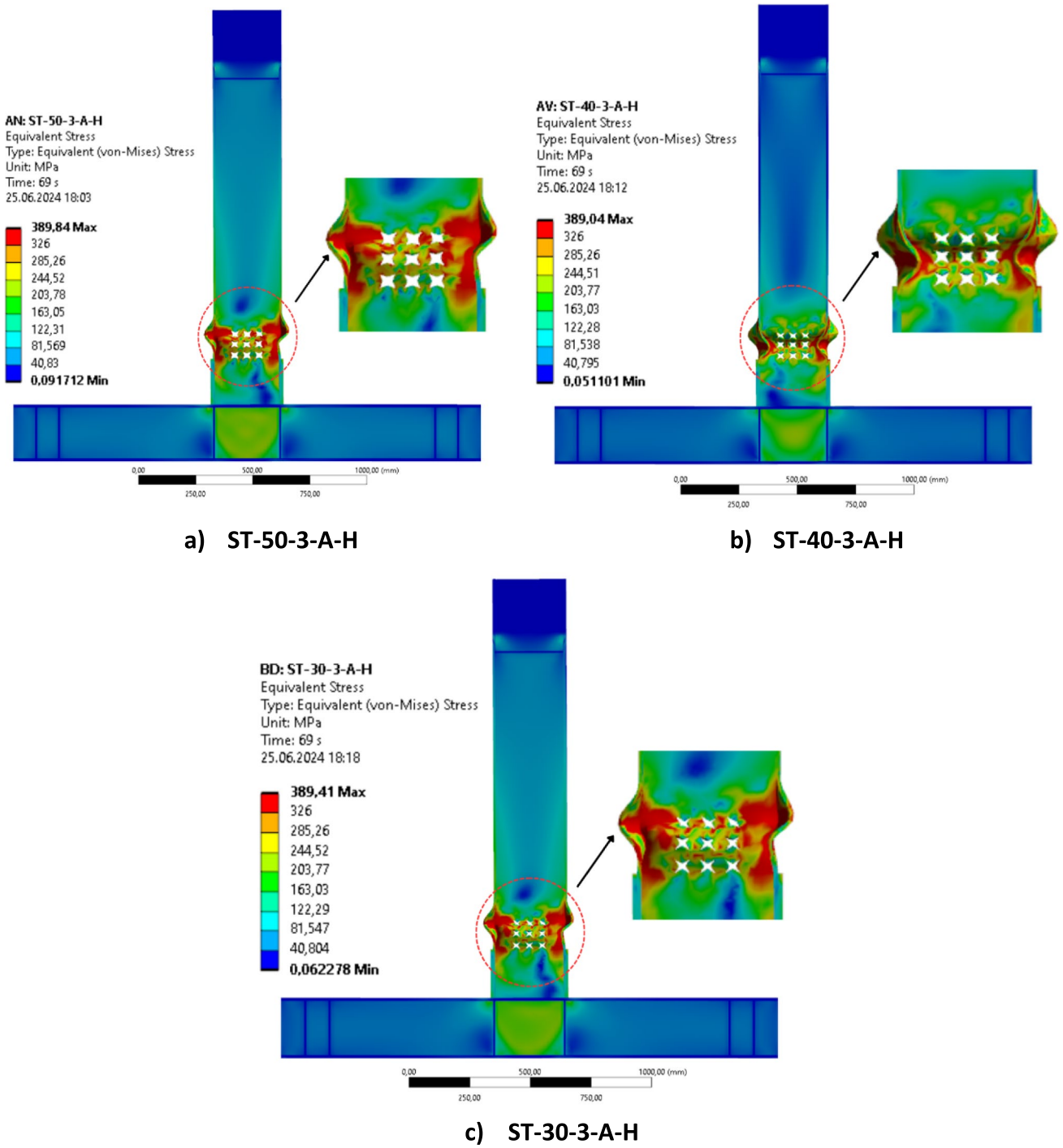

a) ST-50-3-A-H

b) ST-40-3-A-H

c) ST-30-3-A-H

Fig. 12 Top performing auxetic configurations for seismic-resistant steel connections

gradual reduction in strength and stiffness observed in the envelope curves visually demonstrates the failure progression of the connections under cyclic demands, providing a clear visual understanding of how geometric variations in auxetic perforations influence load resistance and deformation capacity.

4.3 Strength and Cyclic Degradation Behaviors

Strength and cyclic degradation are critical parameters in evaluating the seismic reliability of beam-to-column connections. Under repeated lateral loading, structural members may experience progressive reductions in load-bearing

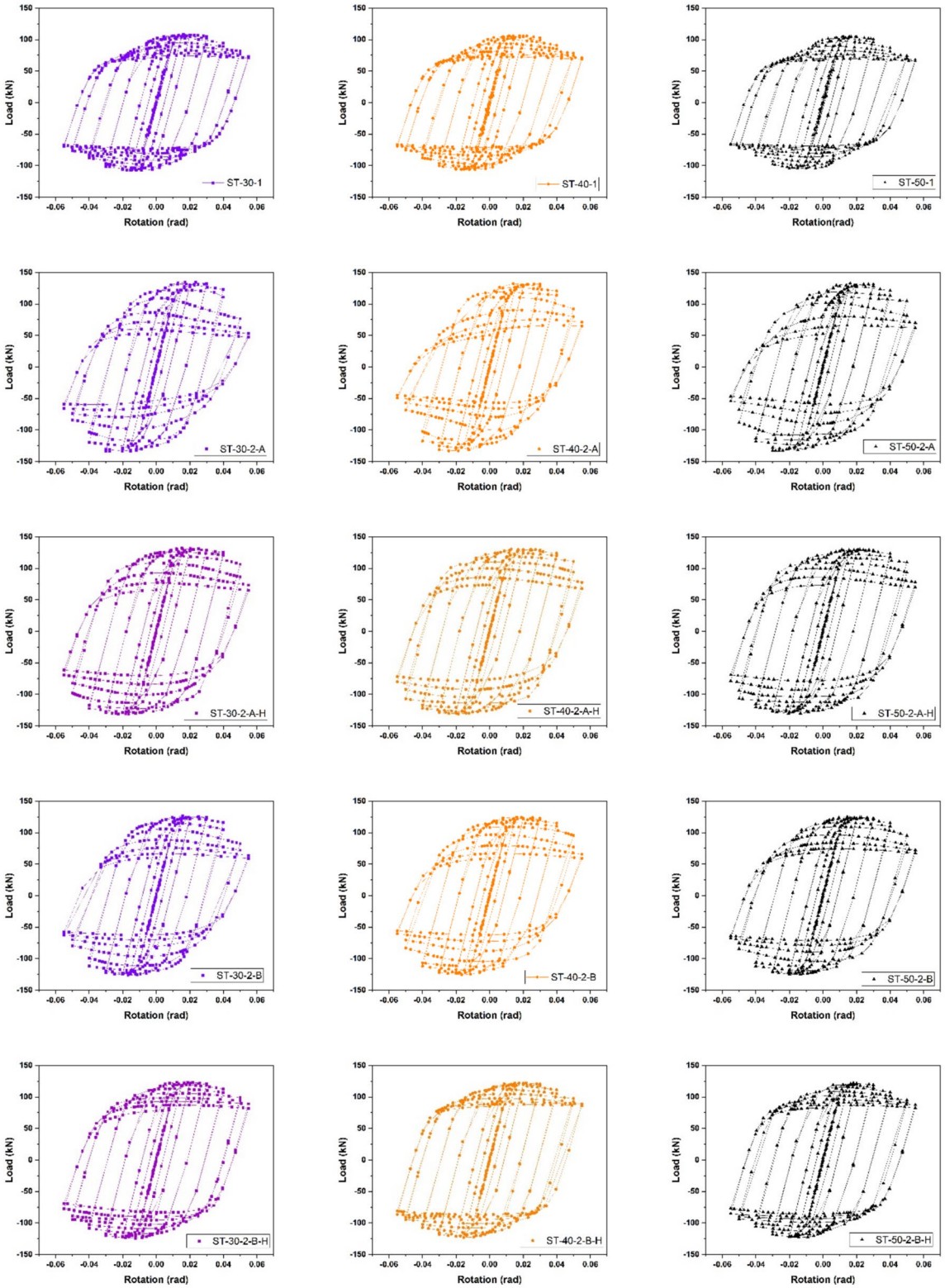

Fig. 13 Hysteretic curve of steel frame connection specimens

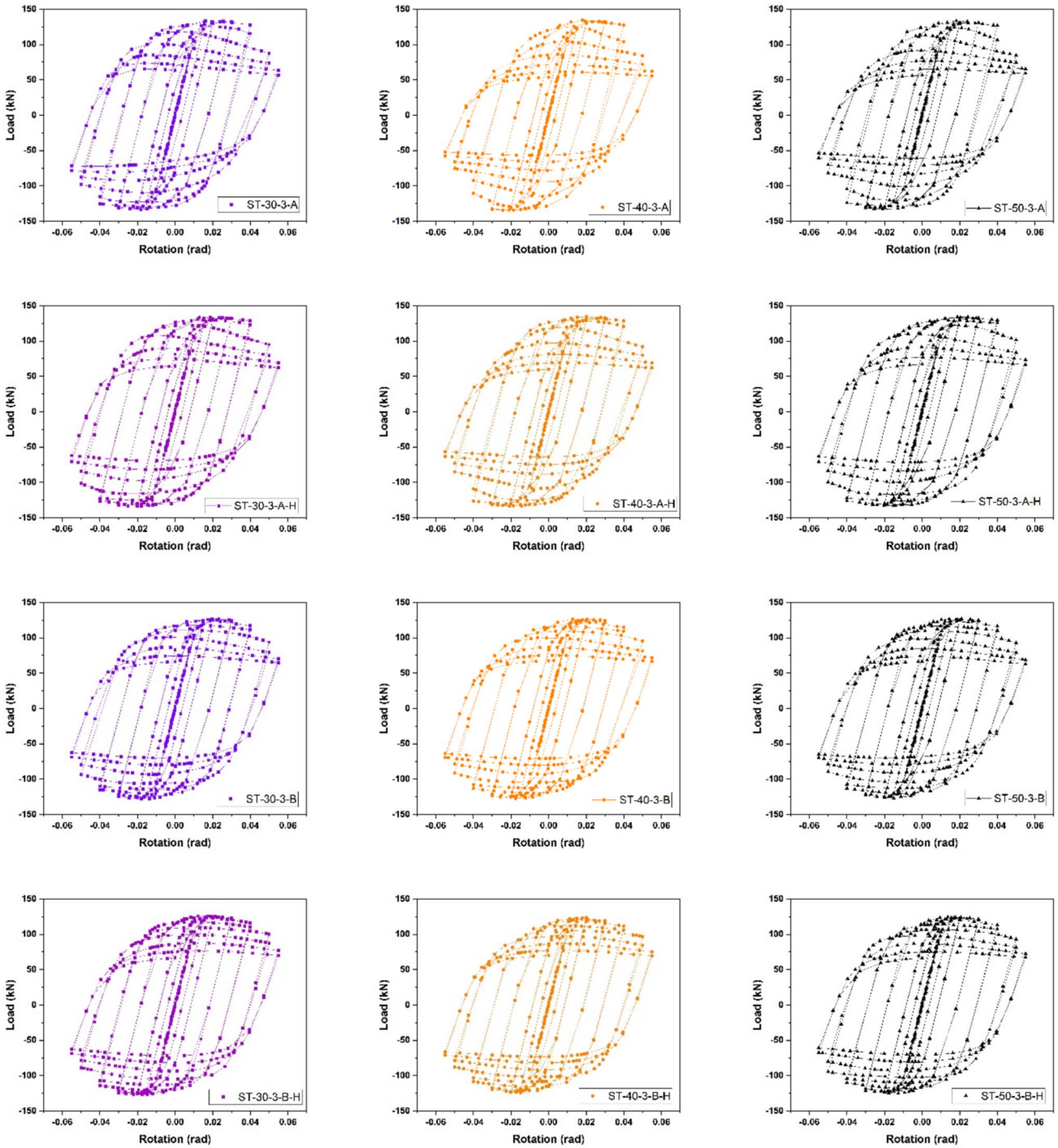

Fig. 13 (continued)

capacity and stiffness due to material fatigue, local buckling, or accumulation of plastic deformation. This degradation directly impacts the shape and area of the hysteresis loop, ultimately influencing the structure's ability to dissipate energy and recover after seismic excitation. To quantify this behavior, characteristic force–displacement values—such as yield strength (P_y), peak strength (P_m), and ultimate strength (P_u), along with their corresponding displacements (Δ_y, Δ_m, Δ_u)—were extracted from the envelope curves, as illustrated in Fig. 15. These values formed the basis for calculating strength degradation ratios and assessing the residual capacity of each auxetic configuration.

Using these parameters, a comparative evaluation was performed for all 27 auxetically perforated connection

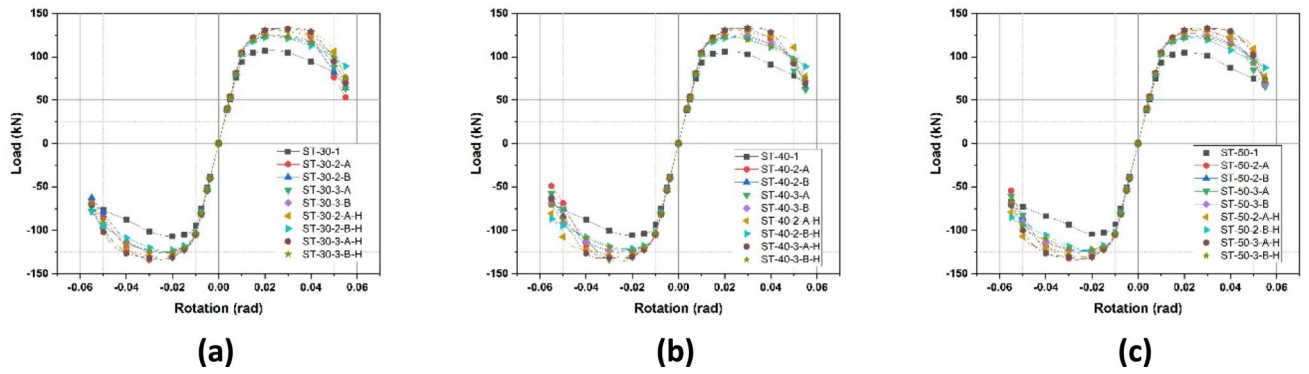

Fig. 14 Comparisons of envelop curve of models. **a** ST-30 groups, **b** ST-40 groups, **c** ST-50 groups

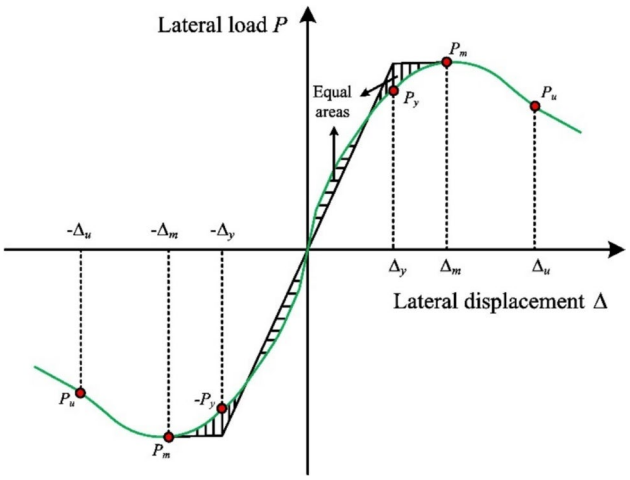

Fig. 15 Defining values of the envelope curve (Xu et al. 2022)

models. The results are presented in Table 4, highlighting their respective peak strengths, ductility capacities, and strength degradation ratios. Among the evaluated designs, the ST-50-3-A-H model recorded the highest peak strength (132.79 kN) and the lowest strength degradation (9.22%), demonstrating superior cyclic stability. The ST-40-3-A-H and ST-30-3-A-H models also exhibited favorable performance, characterized by moderate degradation and high deformation capacity.

The observed performance trend indicates that auxetic geometries with larger star-shaped openings and greater surface engagement improve the connection's ability to dissipate energy and resist degradation. In particular, configurations featuring three perforations (n = 3) with reduced spacing and moderate star angles (30°–50°) were found to delay localized yielding and promote distributed plasticity. These geometric characteristics appear to enhance load redistribution and mitigate stress concentration effects under cyclic loading.

Overall, the results suggest that deliberate adjustment of auxetic parameters—such as the number of perforations, angle, and spacing—can be strategically used to control seismic demand and improve the structural performance of welded steel connections. This supports the broader hypothesis that auxetic pattern integration offers a promising avenue for optimizing energy dissipation and strength retention in seismic-resistant connection design.

During cyclic loading, the rise in the quantity of load cycles causes a progressive growth in cumulative plastic deformation and local buckling deformation of the connection. This ultimately leads to a decrease in the strength of the connection. The cumulative deformation and buckling characteristics of the connection can be partially represented by utilizing the strength degradation ratio of the connection. In this document, the strength degradation ratio of the connection is formulated as follows:

$$\lambda = \frac{P_1^{max} - P_l^{max}}{P_1^{max}} \tag{1}$$

where λ is the strength degradation ratio of connection; P_1^{max} and P_l^{max} were the peak strength of connection in the first cyclic loading and last cyclic loading in the same load step, respectively. To further validate the superior performance of auxetically enhanced connections, the strength degradation behavior of the top-performing ST-50-3-A-H model was compared with that of a conventional welded connection (SJ-8) based on experimental data from Xu et al. (2022). As shown in Fig. 16, the ST-50-3-A-H model exhibited significantly lower strength degradation ratios across successive load steps, maintaining greater structural stability throughout the cyclic loading process. In contrast, the SJ-8 model showed a steeper loss in load-carrying capacity, especially during later loading cycles. This comparative trend reinforces the efficacy of the proposed auxetic geometry in distributing stress, reducing fatigue accumulation, and preserving mechanical performance under seismic demands.

Table 4 Strength and corresponding displacement values for connection

	P_y	P_m	P_u	Δ_y	Δ_m	Δ_u
ST-50-1	92.95	104.42	68.04	17.65	34.36	98.11
ST-50-2-A	104.56	131.05	70.04	17.99	53.58	105.40
ST-50-2-B	102.66	122.74	72.29	17.92	52.81	101.87
ST-50-2-A-H	104.57	128.47	77.76	17.98	53.35	103.83
ST-50-2-B-H	102.62	121.38	87.42	17.91	35.40	98.64
ST-50-3-A	104.90	130.96	65.38	18.00	53.55	109.63
ST-50-3-B	103.59	125.47	68.71	17.94	35.56	106.89
ST-50-3-A-H	104.96	132.79	73.31	17.99	53.45	106.25
ST-50-3-B-H	103.44	123.03	72.54	17.93	35.50	104.95
ST-40-1	92.97	105.56	70.83	17.66	34.43	97.43
ST-40-2-A	104.61	131.44	70.90	17.99	53.58	104.96
ST-40-2-B	102.81	122.90	65.57	17.92	35.43	104.05
ST-40-2-A-H	104.59	128.82	77.54	17.98	53.34	104.67
ST-40-2-B-H	102.54	121.31	88.84	17.90	35.41	98.65
ST-40-3-A	104.93	132.50	61.93	18.00	53.58	111.36
ST-40-3-B	103.44	125.00	71.84	17.94	35.55	104.05
ST-40-3-A-H	104.92	132.72	69.04	17.99	53.43	107.26
ST-40-3-B-H	103.29	123.43	75.05	17.93	35.50	101.37
ST-30-1	93.81	106.81	73.30	17.68	34.52	97.42
ST-30-2-A	104.60	131.93	52.95	17.99	53.56	108.45
ST-30-2-B	102.89	123.55	63.81	17.92	35.46	108.55
ST-30-2-A-H	104.60	129.14	73.28	17.98	53.37	105.35
ST-30-2-B-H	102.75	121.93	89.15	17.91	35.42	99.11
ST-30-3-A	104.93	131.90	63.23	18.00	53.57	110.41
ST-30-3-B	103.67	125.32	70.01	17.95	35.58	105.80
ST-30-3-A-H	104.96	131.84	69.36	17.99	53.45	108.09
ST-30-3-B-H	103.57	123.88	76.77	17.93	35.53	103.76

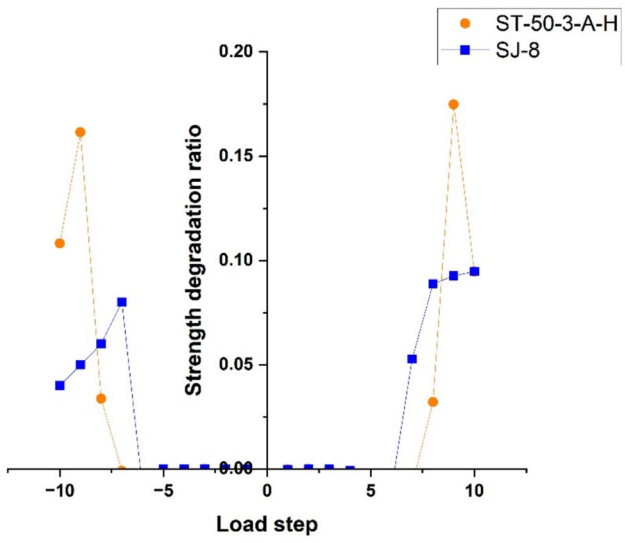

Fig. 16 A comparison of the strength degradation curves for the SJ-1 and ST-50-3-A-H

4.4 Ductility and Rotation Behaviors

The ductility and rotational characteristics of steel connections can be assessed using the displacement ductility coefficient and plastic rotation (Mahin et al. 2002; Xu et al. 2022). In this investigation, we will use the ductility coefficient, elastic rotation, plastic rotation, and total rotation to study the ductility and deformation of the suggested connection, as expressed below:

$$\mu = \frac{\Delta_u}{\Delta_y} \tag{2}$$

$$\theta_e = \frac{\Delta_y}{L} \tag{3}$$

$$\theta_P = \frac{\Delta_u - \Delta_y}{L} \tag{4}$$

$$\theta_t = \theta_e + \theta_p \tag{5}$$

The displacement ductility coefficient (μ) is defined by the ratio of the maximum displacement to the yield displacement. θ_e refers to the elastic rotation, while θ_p represents the plastic rotation. θ_t denotes the total rotation, including both elastic and plastic rotation. Meanwhile, L signifies the calculated length of the beam. Table 5 presents Ductility coefficient and rotations of the connection models.

The ductility and rotation capacity of a connection are critical indicators of its ability to undergo inelastic deformation without experiencing significant strength loss. Among the 27 models examined, the ST-50-3-A-H, ST-40-3-A-H, and ST-30-3-A-H configurations exhibited the most favorable performance. Specifically, the ST-50-3-A-H model achieved a ductility coefficient of 6.09 and a total rotation capacity of 6.26 radians, while the ST-30-3-A-H model reached the highest total rotation capacity at 6.31 radians, despite having a slightly lower ductility coefficient (6.13). The ST-40-3-A-H model balanced both indicators with a ductility coefficient of 6.19 and rotation capacity of 6.24.

As illustrated in Fig. 17, the contributions of elastic and plastic deformation to the total rotation were substantial,

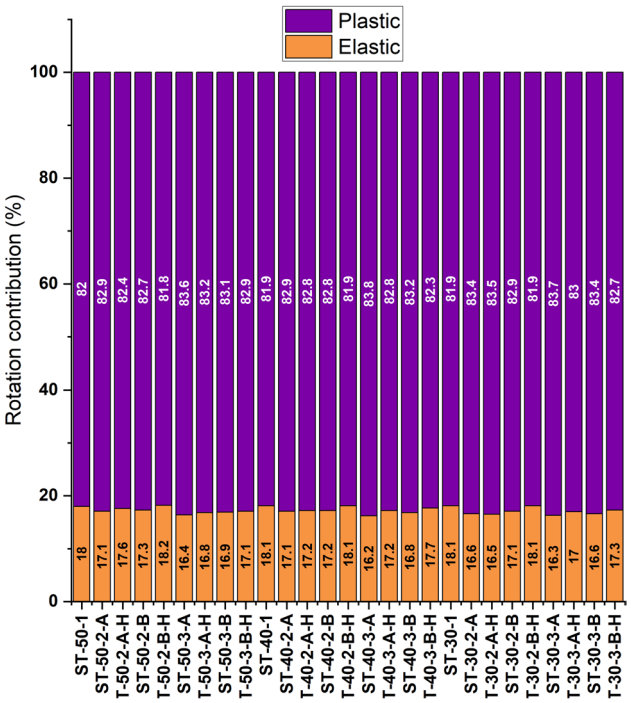

Fig. 17 Contribution between elastic and plastic deformation

Table 5 Ductility coefficient and rotations of the connection models

	μ	θ_e	θ_p	θ_t
ST-50-1	5.56	1.01	4.60	5.61
ST-50-2-A	5.86	1.03	4.99	6.02
ST-50-2-B	5.69	1.02	4.80	5.82
ST-50-2-A-H	5.78	1.03	4.91	5.93
ST-50-2-B-H	5.51	1.02	4.61	5.64
ST-50-3-A	6.09	1.03	5.24	6.26
ST-50-3-B	5.96	1.03	5.08	6.11
ST-50-3-A-H	5.91	1.03	5.04	6.07
ST-50-3-B-H	5.85	1.02	4.97	6.00
ST-40-1	5.52	1.01	4.56	5.57
ST-40-2-A	5.83	1.03	4.97	6.00
ST-40-2-B	5.81	1.02	4.92	5.95
ST-40-2-A-H	5.82	1.03	4.95	5.98
ST-40-2-B-H	5.51	1.02	4.61	5.64
ST-40-3-A	6.19	1.03	5.33	6.36
ST-40-3-B	5.80	1.02	4.92	5.95
ST-40-3-A-H	5.96	1.03	5.10	6.13
ST-40-3-B-H	5.65	1.02	4.77	5.79
ST-30-1	5.51	1.01	4.56	5.57
ST-30-2-A	6.03	1.03	5.17	6.20
ST-30-2-B	6.06	1.02	5.18	6.20
ST-30-2-A-H	5.86	1.03	4.99	6.02
ST-30-2-B-H	5.53	1.02	4.64	5.66
ST-30-3-A	6.13	1.03	5.28	6.31
ST-30-3-B	5.90	1.03	5.02	6.05
ST-30-3-A-H	6.01	1.03	5.15	6.18
ST-30-3-B-H	5.79	1.02	4.90	5.93

indicating that these connections were capable of sustaining large plastic rotations prior to failure. The enhanced ductility observed in the 3-A series is attributed to their optimized auxetic geometry, which facilitates distributed yielding and delays the onset of localized damage. These characteristics are essential for ensuring post-yield stability and energy absorption during seismic events.

4.5 Energy Dissipation

The total energy dissipation (E_{total}) is a key indicator of a connection's capacity to absorb and release seismic energy through inelastic deformation. It is calculated by summing the areas enclosed by the hysteresis loops of the cyclic loading response. Higher energy dissipation indicates enhanced resilience under earthquake loading, reducing the likelihood of brittle failure and improving the damping characteristics of the structural system.

To evaluate the performance enhancement offered by auxetic geometries, all parametric models were compared to the conventional SJ-8 welded connection in terms of their cumulative energy dissipation. This comparison provides insight into the relative effectiveness of different auxetic configurations in absorbing seismic energy.

ST-50 Series: As shown in Fig. 18, all ST-50 models outperformed the SJ-8 baseline in terms of energy dissipation. The ST-50-1 model showed a modest increase of 1.99%, while ST-50-2-A and ST-50-2-B exhibited more notable

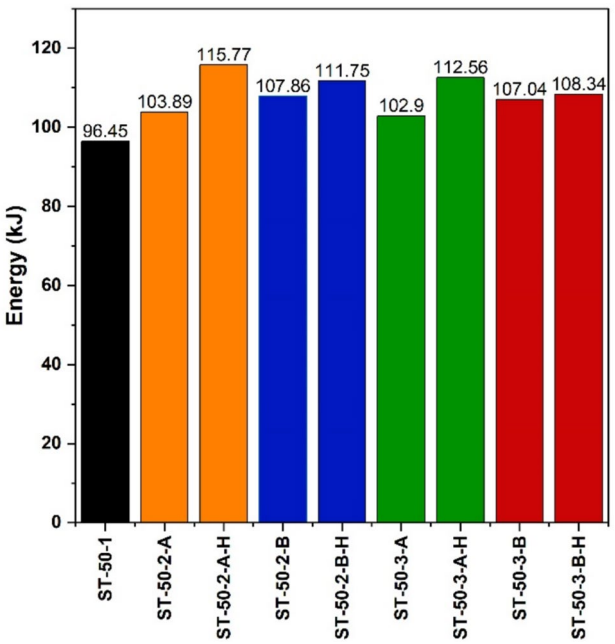

Fig. 18 Energy dissipation of ST-50 models

improvements of 9.85% and 14.03%, respectively. Models incorporating reduced spacing between stars—ST-50-2-A-H and ST-50-2-B-H—achieved even greater gains of 22.41% and 18.18%, respectively. Other ST-50 series models demonstrated increases ranging from 8.81% to 18.99%. These results suggest that auxetic configurations with higher surface engagement and denser star distribution significantly enhance the energy dissipation capacity of the connection.

ST-40 Series: A similar pattern was observed in the ST-40 group, as illustrated in Fig. 19. The ST-40-1 model showed a 4.99% increase over SJ-8, while ST-40-2-A and ST-40-2-B achieved 4.16% and 9.30%, respectively. Once again, halved spacing in ST-40-2-A-H and ST-40-2-B-H models resulted in marked improvements of 21.75% and 19.30%. Other models in this series exhibited energy dissipation increases between 4.65% and 14.06%, affirming the positive correlation between perforation density and seismic energy absorption.

ST-30 Series: Fig. 20 presents the results for ST-30 models. The ST-30-1 model exceeded the SJ-8 reference by 6.76%, while ST-30-2-A and ST-30-2-B increased by 4.70% and 6.80%, respectively. Denser configurations ST-30-2-A-H and ST-30-2-B-H yielded the most significant improvements, with 18.84% and 19.08% gains. Other ST-30 variants reported enhancements in the range of 13.64% to 16.59%, again highlighting the role of perforation layout in dictating energy dissipation behavior**.**

These findings clearly demonstrate that auxetically holed welded connections outperform conventional designs in terms of energy dissipation, particularly when star geometry is optimized via increased quantity and reduced spacing. The results underscore the potential of auxetic geometries to act as engineered energy absorbers in seismic-resistant design, offering both ductility and resilience without compromising connection integrity.

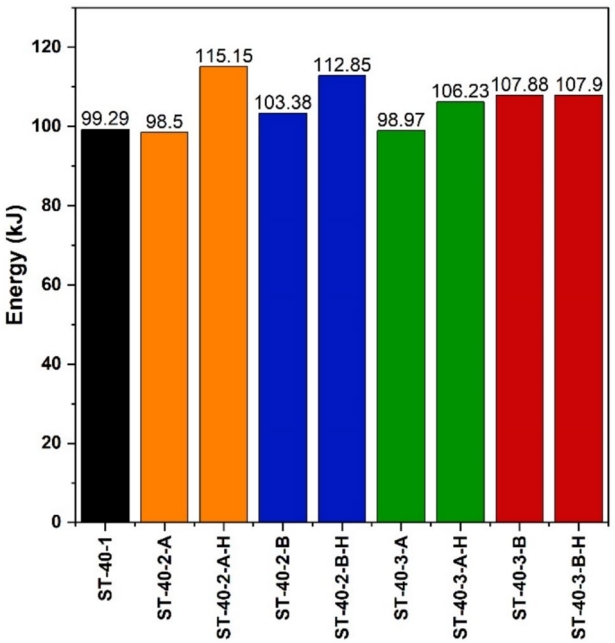

Fig. 19 Energy dissipation of ST-40 models

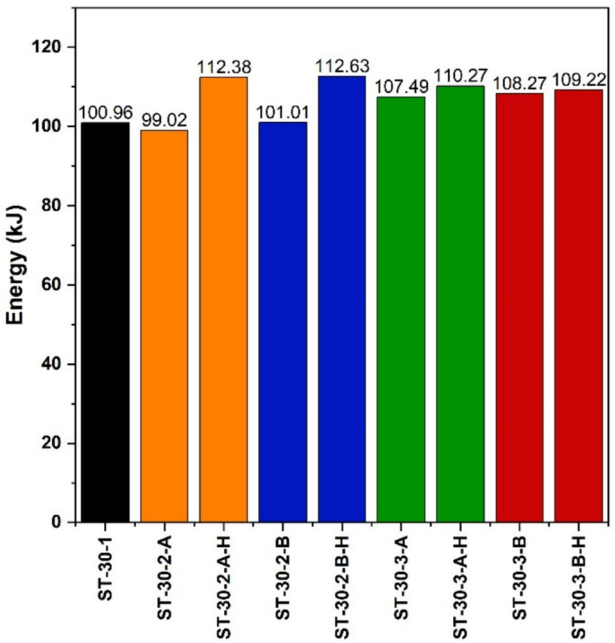

Fig. 20 Energy dissipation of ST-30 models

5 Summary and Conclusions

This study introduced a novel welded beam-to-column connection concept incorporating *star-shaped auxetic perforations* in the beam web to improve seismic performance. A total of 27 finite element models were developed with varying geometric configurations, including star angle, perforation area, spacing, and number of openings. These models were validated against experimental results from the SJ-8 connection and evaluated under FEMA-350 cyclic loading protocols. The performance of each configuration was assessed in terms of strength, ductility, rotation capacity, energy dissipation, and strength degradation.

Key findings of the study can be summarized as follows:

- *Strength and Cyclic Stability*: The ST-50-3-A-H model exhibited the highest peak strength (132.79 kN) and the lowest degradation (9.22%), demonstrating superior cyclic resilience. Other configurations such as ST-40-3-A-H and ST-30-3-A-H also showed balanced strength and deformation characteristics.
- *Ductility and Rotation Capacity*: The top-performing models achieved ductility coefficients above 6.0 and rotation capacities exceeding 6.2 radians, satisfying requirements for special moment frames. Reduced spacing between auxetic perforations (d/2) contributed significantly to plastic rotation enhancement.
- *Energy Dissipation*: All auxetic-enhanced models surpassed the SJ-8 baseline in energy dissipation capacity. The most significant gains were observed in "-H" models with higher perforation density, confirming the effectiveness of auxetic layouts in absorbing seismic energy.
- *Geometric Optimization*: Parametric evaluation revealed that models with three star-shaped openings (n = 3), moderate star angles (30°–50°), and minimized spacing provided the best trade-off between strength retention and deformation control.

Overall, the study confirms that integrating auxetic geometries into welded steel connections significantly improves seismic performance by enhancing energy dissipation, increasing ductility, and reducing degradation. The findings offer a new design strategy for high-performance steel moment connections in earthquake-prone regions.

Future research should focus on the experimental validation of these configurations under full-scale testing, as well as the inclusion of additional variables such as residual drift, low-cycle fatigue behavior, and manufacturability constraints. The practical applicability of auxetic-based structural systems also warrants investigation through full-building simulations and cost-performance analyses.

Acknowledgements The research described in this paper was financially supported by Ataturk University (Project No: FDK-2024-13847).

Author Contributions Oguzhan Akarsu: Methodology, Investigation, Visualization, Formal analysis, Conceptualization, Writing. Abdulkadir Cüneyt Aydın: Validation, Supervision, Project administration, Methodology, Writing. Declaration of competing interest The author declares that there is no conflict of interest regarding the publication of this paper. Data availability All the data generated and used in the current study is available in the manuscript.

Data Availability No datasets were generated or analysed during the current study.

Declarations

Conflict of interest The authors declare no competing interests.

References

Alomarah A, Masood SH, Ruan D (2022) Dynamic and quasistatic properties of an auxetic structure: a comparative study. Adv Eng Mater 24(9):2101811

An B, Hu Z, Mao N, Tian W (2018). Seismic ductility capacity research of integral building-bridge station structure. In: IOP conference series: earth and environmental science, vol 189(2). IOP Publishing, p 022056

Bagewadi SS, Bhagchandani RK (2023) Effect of gradient structure on additively manufactured auxetic and hybrid auxetic structure for energy absorption applications. Proc Inst Mech Eng Part l J Mater des Appl 237(8):1739–1751

Bishay-Girges NW (2020) Improved steel beam-column connections in industrial structures. Eng Technol Appl Sci Res 10(1):5126–5131

Bohara RP, Linforth S, Nguyen T, Ghazlan A, Ngo T (2023) Anti-blast and-impact performances of auxetic structures: a review of structures, materials, methods, and fabrications. Eng Struct 276:115377

Braconi A, Salvatore W, Tremblay R, Bursi OS (2007) Behaviour and modelling of partial-strength beam-to-column composite joints for seismic applications. Earthq Eng Struct Dyn 36(1):142–161

Chung KF, Liu TCH, Ko ACH (2001) Investigation on Vierendeel mechanism in steel beams with circular web openings. J Constr Steel Res 57(5):467–490

Elkady A, Lignos DG (2014) Modeling of the composite action in fully restrained beam-to-column connections: implications in the seismic design and collapse capacity of steel special moment frames. Earthq Eng Struct Dyn 43(13):1935–1954

Guo Z, Huang SS (2016) Behaviour of restrained steel beam with reduced beam section exposed to fire. J Constr Steel Res 122:434–444

Han LH, Li W (2010) Seismic performance of CFST column to steel beam joint with RC slab: Experiments. J Constr Steel Res 66(11):1374–1386

Hassanin H, Abena A, Elsayed MA, Essa K (2020) 4D printing of NiTi auxetic structure with improved ballistic performance. Micromachines 11(8):745

Hu S, Liu S, Zeng S, Zhang B, Xu Z (2025) Investigating seismic performance of a novel self-centering shear link in EBF utilizing experimental and numerical simulation. J Constr Steel Res 224:109129

Li Y, Huang B (2022) Evaluation on seismic performance of beam-column joints of fabricated steel structure with replaceable energy-dissipating elements. Sustainability 14(6):3350

Liu Y, Zhao C, Xu C, Ren J, Zhong J (2023) Auxetic meta-materials and their engineering applications: a review. Eng Res Express 5(4):042003

Liu S, Chen S, Zeng S, Zhang B, Hu S (2025) Seismic performance analysis of K-shaped EBF with an innovative crack-resistant composition beam. J Build Eng 101:111818

Mahin S, Malley J, Hamburger R (2002) Overview of the FEMA/SAC program for reduction of earthquake hazards in steel moment frame structures. J Constr Steel Res 58(5–8):511–528

Mahmoud H, Turbert C (2014) Numerical Assessment of connections with reduced beam sections under fire following an earthquake using continuously updated boundary condition. In: Structures Congress 2014, pp 1138–1147

Miller DK (1998) Lessons learned from the Northridge earthquake. Eng Struct 20(4–6):249–260

Mojaver M, Azdast T, Hasanzadeh R (2024) An experimental and numerical study on an innovative metastructure for 3D printed thermoplastic polyurethane with auxetic performance. Polym Adv Technol 35(2):e6298

Muguruma H, Nishiyama M, Watanabe F (1995) Lessons learned from the Kobe earthquake—a Japanese perspective. PCI J 40(4):28–42

Nguyễn H, Fangueiro R, Ferreira F, Nguyễn Q (2023) Auxetic materials and structures for potential defense applications: an overview and recent developments. Text Res J 93(23–24):5268–5306

Rose S, Siu D, Zhu J, Roufail R (2023) Auxetics in biomedical applications: a review. J Minerals Mater Charact Eng 11:27–35

Sofias C, Tzourmakliotou D (2018) Reduced beam section (RBS) moment connections-analytical investigation using finite element method. Civ Eng J 4(6):1240–1253

Tsavdaridis KD, D'Mello C (2012) Vierendeel bending study of perforated steel beams with various novel web opening shapes through nonlinear finite-element analyses. J Struct Eng 138(10):1214–1230

Tsavdaridis KD, Faghih F, Nikitas N (2014) Assessment of perforated steel beam-to-column connections subjected to cyclic loading. J Earthq Eng 18(8):1302–1325

Venture SJ, Guidelines Development Committee (2000) Recommended seismic design criteria for new steel moment-frame buildings, vol 350. Federal Emergency Management Agency, Washington

Wang Z, Hu H (2014) Auxetic materials and their potential applications in textiles. Text Res J 84(15):1600–1611

Wang Y, Zeng H, Nie B, Jia F, Gao Q (2024) Energy absorption characteristics of carbon fiber reinforced plastic/aluminum hybrid materials double arrow-head auxetic structure. J Sandwich Struct Mater 26(4):490–506

Xu Q, Chen H, Li W, Zheng S, Zhang X (2022) Experimental investigation on seismic behavior of steel welded connections considering the influence of structural forms. Eng Fail Anal 139:106499

Yang Q, Li B, Yang N (2009) Aseismic behaviors of steel moment resisting frames with opening in beam web. J Constr Steel Res 65(6):1323–1336

Zhang J, Lu G, Ruan D, Wang Z (2018) Tensile behavior of an auxetic structure: analytical modeling and finite element analysis. Int J Mech Sci 136:143–154

Zhang X, Zheng S, Zhao X (2019) Seismic performance of steel beam-to-column moment connections with different structural forms. J Constr Steel Res 158:130–142

Zhang Q, Zhu Y, Wang Y, Li J (2023) A novel Barbell-shaped perforated auxetic metastructure with superior auxetic effect. Phys Status Solidi (b) 260(12):2300351

Zhao LY, Guo D, Yang YQ, Diao YS, Liu XL (2024) Seismic performance and replaceability of steel frame structures with replaceable beam segments. Adv Steel Constr 20(1):69–80

Zhuohong Z (2020) Chiral auxetics as a protective material. Master's thesis. National University of Singapore, Singapore